Effect of Hydrodynamics on Reactive Mixing in Laminar Flows

E. S. Szalai, J. Kukura, P. E. Arratia, and F. J. Muzzio
Dept. of Chemical and Biochemical Engineering, Rutgers University, Piscataway, NJ 08854

The effects of diffusion and convection on the evolution of reactions in chaotic flows are examined. Direct numerical simulations are applied to compute the evolution of the mixing structure, describe the stretching field, and solve the convection-reaction-diffusion material balance in a periodic, 2-D chaotic flow with an instantaneous, bimolecular reaction: $A + B \rightarrow 2P$. These computations demonstrate that the location of the reactive zones in the flow can be predicted from the stretching field. The time-evolution of the concentration profiles approaches an invariant shape when the time scale of the convective and diffusive mixing processes are comparable. Under such conditions, exponential stretching and its consequence, asymptotic directionality, are the mechanisms controlling the evolution of chaotic reactive systems.

Introduction

The effects of flow and mixing on reactive systems have been recognized for many decades, yet the interplay of convection and diffusion has traditionally been treated with overly simplistic approaches. The complexity of applications where both diffusion and mechanical stirring occur simultaneously with reactions has been overwhelming to the point that, perhaps in despair, critical aspects of convective flow have been altogether neglected. The classic approach of drawing a black box around the reactor and examining only the intrinsic kinetics of the reactive process is only meaningful when macroscopic inhomogeneities can no longer be detected. This method treats the intrinsic kinetics properly, but can only give insight for processes with slow reactions. It is bound to fail when reactions occur faster than the time scale for homogenization in the system. Not only do we run the risk of overestimating the selectivity and conversion during the design process (a typical problem during reactor scale-up), but completely ignore that a "well-mixed", homogeneous state may never be reached during the entire life of the process.

Chaotic flows have been proven to be the only effective route to destroy segregation rapidly in viscous mixing applications, which are particularly prone to remain inhomogeneous for long periods of time (Lamberto et al., 1996; Avalosse and Crochet, 1997; Hobbs et al., 1997; Unger and Muzzio, 1999). In the past two decades, the effect of chaotic mixing without reactions has been examined in a variety of increasingly complex mixer geometries on a case-by-case basis. However, without a deep understanding of how fluid motion couples with diffusion and molecular kinetics in reactive flows, we cannot yet take the leap to include all transport mechanisms in a realistic geometry. Simplifications have been made by considering only the effects of diffusion and reaction without convection, or treating convection as if it was uniform throughout the mixing domain. Only a handful of publications have considered the combined effect of chaotic convection and diffusion in a reactive mixing application (Muzzio and Ottino, 1988; Metcalfe and Ottino, 1994; Ottino, 1994; Muzzio and Liu, 1996; Zalc and Muzzio, 1999). These investigations established that the local rate of mixing affects the progression of the reaction in the chaotic flow. A distinctive similarity between the product concentration field and the mixing structure is observed, but relationships between the mixture topology and its effects on the dynamics of the reaction has not yet been established.

Chaotic mixing produces complex, layered structures that appear to be a collection of different-size filaments filling the chaotic region. The two controlling mechanisms of the convective mixing process, stretching and folding, occur simultaneously at different rates in each portion of the flow, creating complex patterns. An example is shown in Figure 1. The figure shows the cross-section of a laboratory-scale mixing vessel agitated with a single Rushton impeller. The shaft is on

Correspondence concerning this article should be addressed to F. J. Muzzio.

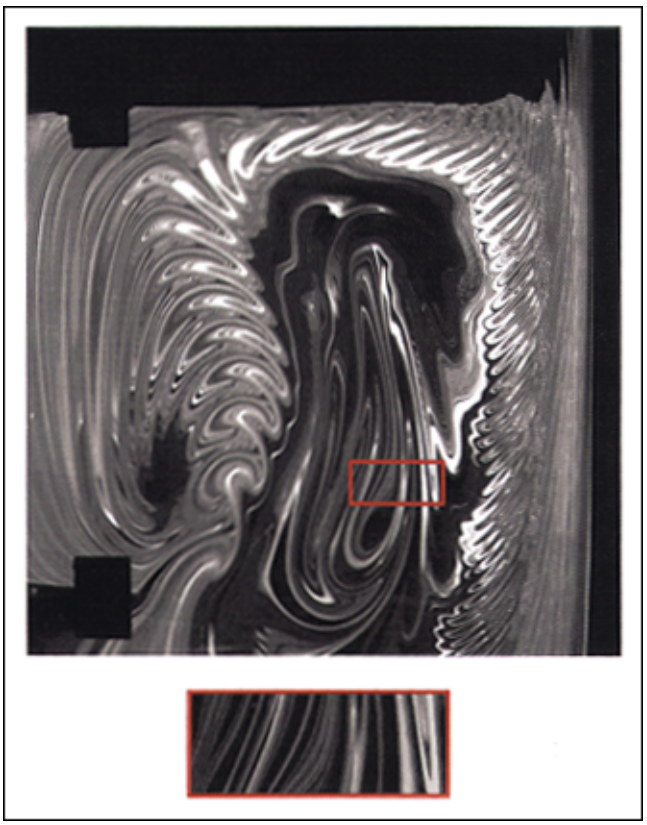

Figure 1. Lamellar mixing structure in a three-impeller stirred tank.

the lefthand side and one of the impeller blades is aligned with the viewing plane in the lower lefthand side corner. In this experiment, fluorescent, pH-sensitive dye is injected into a vessel initially filled with clear glycerine. A laser sheet is passed through the mid-plane of the tank, aligned with the shaft and one of the impeller blades, to illuminate a portion of the fluid. This technique reveals a two-dimensional (2-D) slice of the mixing structure, where the 2-D view promotes visual clarity. Some features highlighted in this experiment are universal to all chaotic mixing applications. The dye, initially injected near the impeller, is rapidly spread throughout the chaotic region of the flow and forms a beautiful, highly filamented, heterogeneous structure. The repetitive layers form as the impeller blades create new folds each time they pass by the viewing plane. The horseshoe-like folds travel towards the walls, deform further, stretch and fold, and eventually recirculate again through the impeller region.

The dye, which is pH sensitive, reveals the location of an instantaneous acid-base reaction occurring at the fluid-fluid interface. The bright sections of the figure are the product-rich areas, where the reaction has been completed. The dark regions are slower mixing areas, where the clear acidic glycerine and the dye-laced basic glycerine have not yet come into contact with each other. The interplay of three fundamental mechanisms, convective mixing, diffusion, and reaction, creates the peculiar landscape shown in Figure 1. This type of landscape is not unique to the stirred tank and has been observed experimentally in other systems (Rothstein et al., 1999). It is important to examine the combined effect of the three components to explain how chemical reactions are influenced by the hydrodynamics. If we magnify a small portion of the dye filament, we can focus on the local interaction between stretching, diffusion, and reaction. This experimental observation is the basis of a traditional approach to laminar reactive mixing problems, the "lamellar model," which views the system as a composite of parallel 1-D lamellae (Ottino et al., 1979; Ottino, 1982). Several numerical and analytical studies have examined the diffusion-reaction equation in such a "1-D" system, assuming that convection has already pre-organized the striations in an alternating pattern during a pre-mixing step (Galfi and Racz, 1988; Muzzio and Ottino, 1989a,b; Muzzio and Ottino, 1990; Taitelbaum et al., 1991, 1992, 1996; Schenkel et al., 1993; O'Shaughnessy and Vavylonis, 2000). In all of these studies the initial distribution of lamellae represents the state of the system at the moment when mechanical agitation is presumably stopped and both diffusion and reaction is turned on (activated by thermal or light energy, for instance). Other investigations, which include the convective stretching in the 1-D model, have found that the initial distribution of striations (hence, the convective mixing step) strongly affects the final outcome of the process (Angst et al., 1982; Chella and Ottino, 1984; Fields and Ottino, 1987; Kusch and Ottino, 1989; Sokolov and Blumen, 1991, 1992; Sokolov et al., 1994).

In this article we take a fresh look at reactive chaotic flows by starting with the simplest case: the interplay of convection, diffusion, and reaction in a *single* fluid lamella surrounded by large neighbors. The 1-D model is described in detail in the following section. Subsequently, we explore 2-D and 3-D scenarios, where the investigation is extended to reactive chaotic flows in two dimensions using an analytically solvable model flow as a case study. It is shown in this section that self-similar phenomenon controls the evolution of concentration distributions in the model system. The analysis is extended to 3-D systems, showing (mainly by analogy) that the simple models described in the previous sections predict important aspects of 3-D reactive mixing. Finally, conclusions and future directions are presented.

Diffusion, Reaction, and Convection in 1-D Systems: A Single Lamella

Let us start with the basics and examine a single reactive fluid element during the chaotic mixing process. Envisioning binary fluid mixtures as a collection of parallel lamellae, we define the characteristic length scale as the thickness of an individual striation (see enlarged window in Figure 1). Figure 2 describes the effect of transport processes in this simplified model. Each striation is made of fluid A or B with initially uniform concentration, distributed in space in an alternating fashion. Convective flow is applied as a locally-uniform stretching process, which elongates striations in one direction while diffusion acts on the striations simultaneously in the orthogonal direction. In a reactive flow, diffusion must occur concurrently with stretching to bring about intimate contact between the reacting mixture components. The effect of diffusion on a concentration profile is dilution of the reactant as the striation becomes wider. Stretching competes with diffusion by concentrating the reactant while contracting the stria-

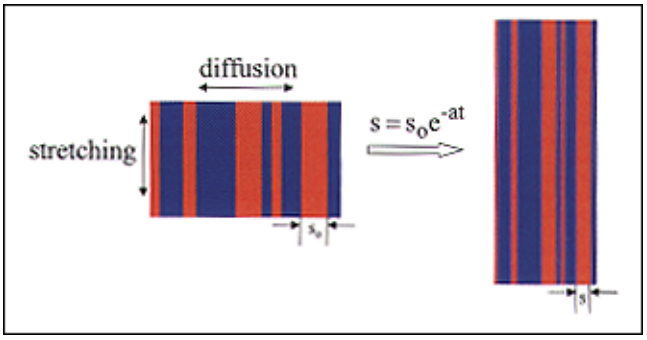

Figure 2. Lamellar model as a simplified approach to reactive mixing flows.

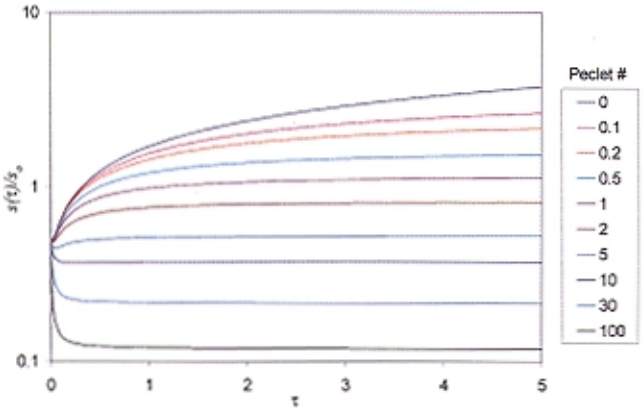

Figure 3. Width of a single lamella approaching a constant with uniform stretching and diffusion.

tion. In this section, we illustrate two important facts: (i) The competition of stretching and diffusion for a single striation of species A surrounded by larger neighbors of species B reaches a balance resulting in a constant profile width; (ii) the concentration profiles under both nonreactive and reactive conditions evolve towards an invariant Gaussian distribution. Later in this article, these attributes of the 1-D model will help us understand behavior in more complex systems.

The species conservation equation for the 1-D lamellar model (Ranz, 1979) is

$$\frac{\partial C_i}{\partial t} - ax\frac{\partial C_i}{\partial x} = D\frac{\partial^2 C_i}{\partial x^2} + R_i, \qquad (1)$$

where x is the spatial coordinate orthodonal to the striation interface, t is time, C_i is the species concentration, D is the diffusion coefficient (constant in the current analysis), R_i is the reaction rate, a is the exponential stretching rate the striation experiences during chaotic convection ($s = s_o\, e^{-at}$), and s_o is the initial width of a single striation (centered at $x = 0$ for the purposes of this work). The stretching rate a is also the topological entropy of the flow (Neufeld and Tel, 1997; Alvarez et al., 1998). In order to simplify the mathematical analysis, the convection term can be eliminated from Eq. 1 by introducing a set of "warped" time (τ) and spatial coordinates (ξ). (The definition of the warped time and spatial coordinates is adapted from previous work (Ranz, 1979; Chella and Ottino, 1984) as

$$\tau = \frac{D}{s_o^2}\int_o^t \frac{dt'}{\exp\left[2\int_0^{t'}\alpha(t'')dt''\right]} \text{ and } \xi = \frac{x}{s(t)}\Bigg).$$

$$\frac{\partial C_A}{\partial \tau} = \frac{\partial^2 C_A}{\partial \xi^2} - \frac{Da_{\mathrm{II}}}{1+2Pe\tau}C_A C_B, \qquad (2)$$

where the Péclet number is $Pe = a/(D/s_o^2)$, and the second Damköhler number is $Da_{\mathrm{II}} = k_r/(D/s_o^2)$, with k_r as the intrinsic reaction rate constant for a second-order reaction between A and B ($A + B \rightarrow 2P$). The first advantage of this transformation is that it reduces the nonreactive system ($Da_{\mathrm{II}} = 0$) to the classic diffusion equation, which has an analytical solution (Crank, 1956). The competition of profile contraction due to stretching with profile expansion due to diffusion can be quantified by performing the reverse-transform of this analytical solution in the warped coordinates to dimensional space.

Without diffusion, a well-defined interface separates neighboring striations and defining their characteristic width at any time is simple. In the finite-reaction and nonreactive cases, defining the characteristic width becomes less trivial, since the diffusing striations become increasingly blurred over time. From here on, we define the width of a single striation surrounded by large neighbors as the distance between locations where the concentration is a specific fraction ($1/\gamma$) of the maximum value at the center of the striation. Using this definition with $\gamma = 2$, Figure 3 graphs the striation width (in dimensional space) vs. time for several Péclet numbers. This graph shows that the width approaches a constant value for all Péclet numbers greater than 0. After sufficient time, the expansion due to diffusion and the contraction due to stretching always achieves a balance. The limiting value of the width is given by $[2\ \ln(\gamma)/Pe]^{0.5}$.

These observations are not restricted to models with a constant stretching rate. Materials in realistic chaotic flows experience a spectrum of stretching intensities depending on their location in the flow. The effect of a nonconstant stretching rate is examined next by introducing a sinusoidal variation in the stretching rate (blue curve in Figure 4). As indicated in Figure 4, changes in the rate of stretching immediately affect the striation thickness. The striation expands and contracts in response to the variations in stretching rate. The red and the green curves in Figures 4a–4b indicate the lower and upper bounds of the width, limited by the amplitude of the oscillations in the stretching rate. If the stretching rate was constant at the minimum or the maximum amplitude, the striation width would approach these bounds and remain constant. However, in response to the varying stretching rate, the striation width changes in a periodic manner with a typical linear first-order dampened response. Comparing Figures 4a–4b, note that the striation expands or contracts depending on the frequency of the oscillations, and never actually reaches a constant width. The higher the frequency of oscillations in the stretching rate, the lower the variation in the width. Despite not approaching an asymptotic limit, striation widths in variable stretching fields are still bounded.

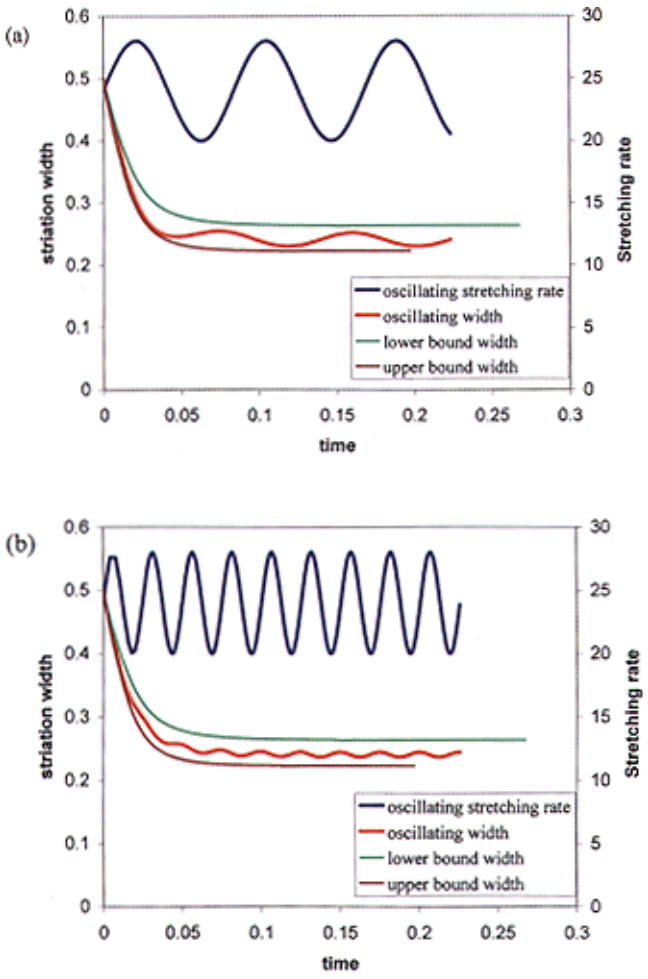

Figure 4. Effect of variable stretching rate on the width of 1-D lamella.

These results have an important implication to more complex, realistic chaotic flows. If only convection occurs, chaotic mixing processes create a very broad spectrum of length scales. Depending on the intensity of stretching at each location in the flow, the striation thickness varies over many orders of magnitude in 2-D and 3-D mixing processes (Alvarez et al., 1998; Szalai and Muzzio, 2002). Diffusion, on the other hand, erases all striations thinner than the lower limit, generating a much narrower (and more realistic) length scale distribution. Knowing the upper and lower bounds of the striation thickness may prove useful for finding the minimum length scale resolution needed to model complex chaotic flows with diffusion.

In order to extend the analysis to reactive systems, let us examine the concentration profiles within a striation. For a reactive striation in the lamellar model, the width of a thin striation surrounded by large neighbors will shrink as the reactant is consumed (as $k_r \to \infty$, the reaction zone approaches a zero thickness moving front). Computation of concentration profiles in the reactive systems reveals a universal shape of the reactant concentration profiles. As the reaction proceeds, concentration profiles approach an invariant shape in both the nonreactive, and infinitely fast and finite-rate reaction cases. Concentration is scaled by the maximum concentration at the center of the striation ($C_{A,\,\mathrm{MAX}}$). The position is scaled by dividing by the width of the striation (or the distance between locations in dimensionless space where the concentration is a specific fraction of the maximum value, designated ξ')

$$C_A^* = \frac{C_A}{C_{A,\mathrm{MAX}}} \quad \text{and} \quad \xi^* = \frac{\xi}{\xi'}, \tag{3}$$

The scaled concentration (C_A^*) is plotted as a function of the scaled position (ξ^*) in Figures 5a, 5b and 5c for a nonreactive case, an infinitely fast reaction case, and a finite rate reaction case ($Pe = 100$, $Da_{\mathrm{II}} = 100$), respectively. As shown in Figure 5, an invariant concentration profile is approached in the scaled coordinates, revealing self-similarity.

Self-similarity is an important trait of the reactive striations, because it indicates that once the concentration distributions acquire the characteristic shape, their evolution can be predicted for future times. Figures 5a and 5c show that the concentration profiles approach a Gaussian shape in the nonreactive and finite rate reaction systems. The infinitely fast reaction is made analogous to the nonreactive case by introducing the variable $\varphi = C_A - C_B$ (Sokolov and Blumen, 1991). With this variable, Eq. 2 is reduced to the classic diffusion equation

$$\frac{\partial \varphi}{\partial \tau} = \frac{\partial^2 \varphi}{\partial \xi^2}, \tag{4}$$

and for the infinitely fast reaction, C_A, C_B, and C_P can be simply recovered from φ

$$\begin{aligned} &\text{If } \varphi > 0 \quad c_A = \varphi, \quad c_P = 1 - \varphi \\ &\text{If } \varphi < 0 \quad c_B = \varphi, \quad c_P = 1 + \varphi. \end{aligned} \tag{5}$$

The Gaussian distribution observed for the scaled concentration profiles in the nonreactive and finite-rate reaction system also applies to φ when it is linearly scaled to span from 0 to 1 by defining $\varphi^* = (\varphi + 1)/2$. The inset of Figure 5b shows the approach of φ^* to the invariant shape.

After identifying the universal shape of the concentration profiles, it is also important to know how much time is required and how much reactant is consumed before striations reach the self-similar regime in the reactive system. It is not particularly useful to know that the process approaches a universal limit if most of the reactive material is consumed by the time the limit is reached in practice.

The overall time evolution of the reaction can be characterized by the conversion. The effects of Da_{II} and Pe on conversion, selectivity, and the location of the reaction interface have been examined previously in 1-D systems (Ranz, 1979; Chella and Ottino, 1984; Taitelbaum et al., 1996). In the current analysis, we measure conversion at the specific point when the concentration within the single striation has reached a self-similar profile. (To determine when the profile achieved the long-term invariant shape, the area between the concentration curve when plotted as C_A^* vs. ξ^* and the

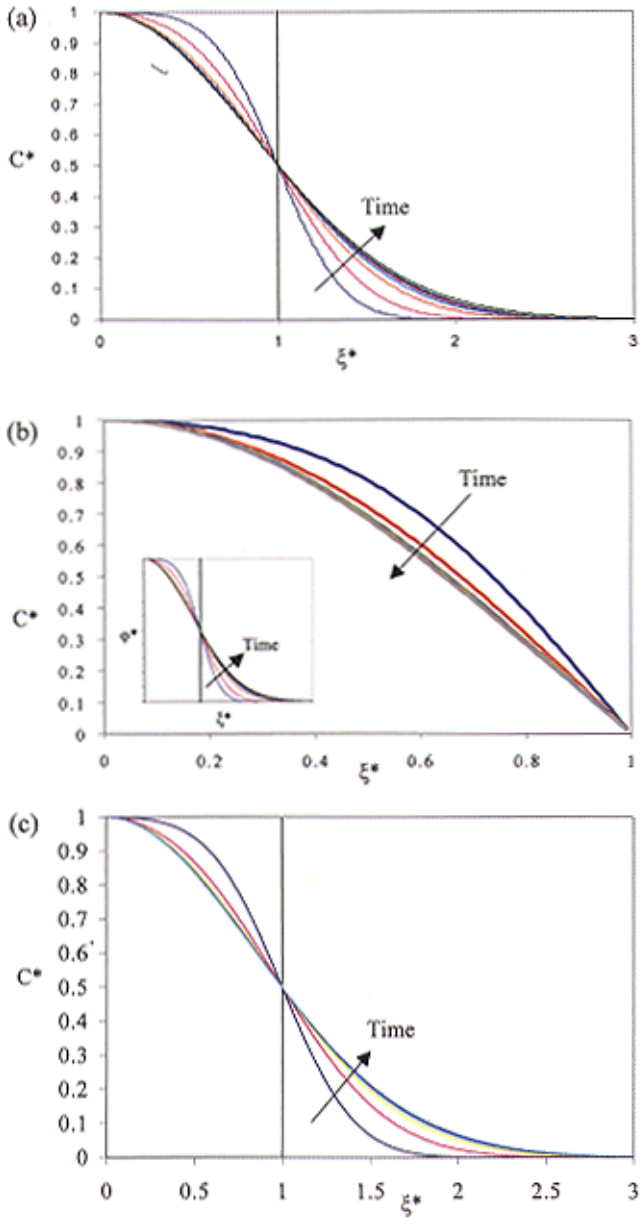

Figure 5. Scaled concentration profiles in a single lamella with an invariant shape: (a) nonreactive case, (b) infinitely fast reaction, and (c) finite reaction.

Inset of (b) reveals how $\varphi = C_A - C_B$ for an infinitely fast reaction is comparable to the concentration profiles.

long-term profile was computed. When this area was less than 2% of the total area under the long-term Gaussian curve, the profile was considered to have obtained the invariant shape.) The conversion for the single striation is defined here as the fraction of A remaining at any given time. Figure 6 shows the conversion required to obtain the invariant profile as a function of Pe and Da_{II}. There is a clear trend of decreasing conversion with increasing Pe at any given value of Da_{II}. This finding is explained by considering that convective transport becomes increasingly fast relative to diffusion as Pe increases. Micromixing is less and less complete at higher values of Pe, which in turn limits the reaction rate. The concentration profiles develop the characteristic self-similar Gaussian shape much faster at higher Pe, indicating the controlling effect of convective mixing on the evolution of the reactive system. The 1-D analysis shows that the interaction of stretching, diffusion, and reaction can achieve a balance that produces time-invariant properties of concentration. Let us now consider what happens in a more complex system, a 2-D chaotic flow.

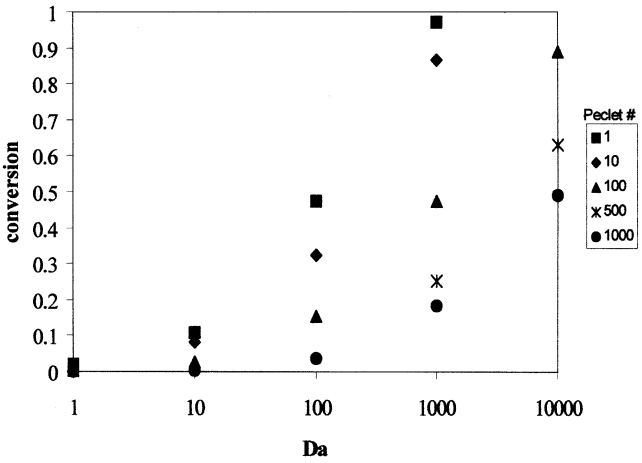

Figure 6. Effect of interplay of reaction, diffusion and convection on the conversion required for a single lamella to achieve the invariant profile shape.

Reactive Chaos in 2-D

A 2-D model flow with spatially distributed stretching rates, "the sine flow," is adopted here as a case study. The flow is created by two sinusoidal velocity fields, where the direction of motion is switched after every half period

$$\begin{matrix}(V_x,V_y) = (\sin 2\pi y, 0) \\ (V_x,V_y) = (0, \sin 2\pi x)\end{matrix} \quad \text{when} \quad \begin{matrix} nT \le t < (n+1/2)T \\ (n+1/2)T \le t < (n+1)T \end{matrix} \tag{6}$$

where T, the flow period, is the only parameter that controls mixing behavior of the flow, n is the number of periods, and t is time. The flow for one period is indicated in Figure 7a. Continuity of the system is assured by enforcing periodic boundary conditions, such that a particle that exits the unit box re-enters through the opposite side. We consider first the evolution of a nonreactive interface between two fluids, which is marked by the thick lines in Figure 7b. Note that the top and bottom face of the unit flow domain are connected and continuous by periodic boundary conditions. Despite its simplicity, this model flow faithfully captures the repertoire of complex mixing behaviors displayed by real world systems, such as static mixers and stirred tanks (Hobbs et al., 1997; Zalc et al., 2001). Similar to physically realizable chaotic flows, large segregated regions are observed at low values of T (that is, $T = 0.8$). As the flow period increases, the system becomes

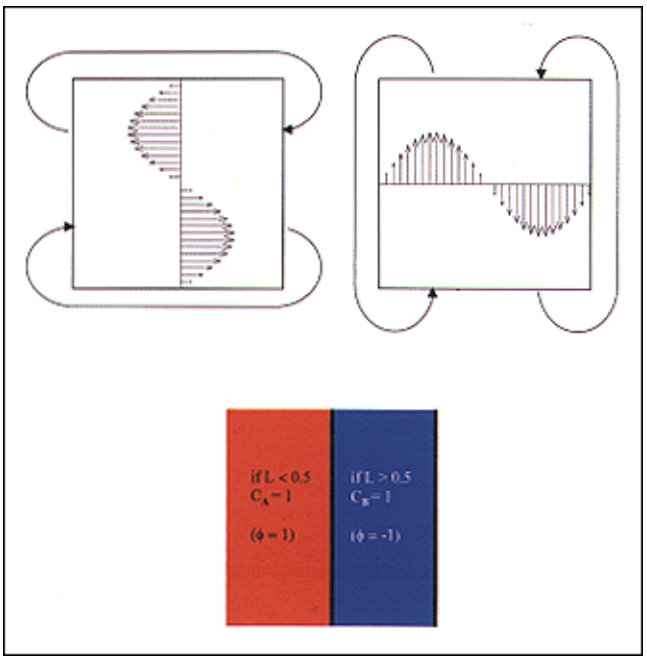

Figure 7. Sine flow model, where an alternating sinusoidal velocity wave induces complex chaotic fluid motion.

almost completely chaotic near $T = 1.6$. Both the asymptotic and short-time mixing behavior of the sine flow in the absence of reaction and diffusion has been examined in previous publication (Alvarez et al., 1998; Muzzio et al., 2000). This work showed that the distribution of stretching values in the sine flow is nearly identical to that of a Kenics static mixer, making it a valuable tool to study flows controlled by chaotic motion.

Let us focus on the specific role of the chaotic flow on the evolution of reactions. The intensity of the convective mixing process is best described by computing the stretching of small vectors as they follow the chaotic flow

$$l_{x,n+1} = l_{x,n} + 2\pi T\left(\cos(2\pi y_n)\right) l_{x,n} \tag{7a}$$

$$l_{y,n+1} = l_{y,n} + 2\pi T\left(\cos(2\pi x_{n+1})\right) l_{y,n+1} \tag{7b}$$

Here, l_x and l_y are the two components of each stretching vector $\underline{l}_{n+1}$, and its magnitude is simply given by $\underline{l}_{n+1} = (l^2_{x,n+1} + l^2_{y,n+1})^{1/2}$. Having a closed-form expression for the stretching field, such as Eqs. 7a and 7b, is extremely useful. The analytical expression for stretching facilitates the development of algorithms for capturing the mixing microstructures with the best possible accuracy over a wide distribution of length scales. Figure 8 shows the stretching field in the sine flow for three consecutive periods, $n = 1$, 2 and 3 for $T = 1.6$ (nearly globally chaotic flow). Due to the extremely wide distribution of stretching values in chaotic flows, a logarithmic color scale is best suited to display the results. For these computations, we placed $(1{,}040 \times 1{,}040)$ vectors in the flow over a uniform x, y lattice. Each vector had an initial length of $(l_{xo};\ l_{yo}) = (0\ ;\ 1)$. The figure demonstrates that a characteristic stretching field emerges within the first two periods, remaining self-similar at any later time. The location of low and high stretching manifolds remains invariant in the flow, except for increasingly finer details that appear at later times.

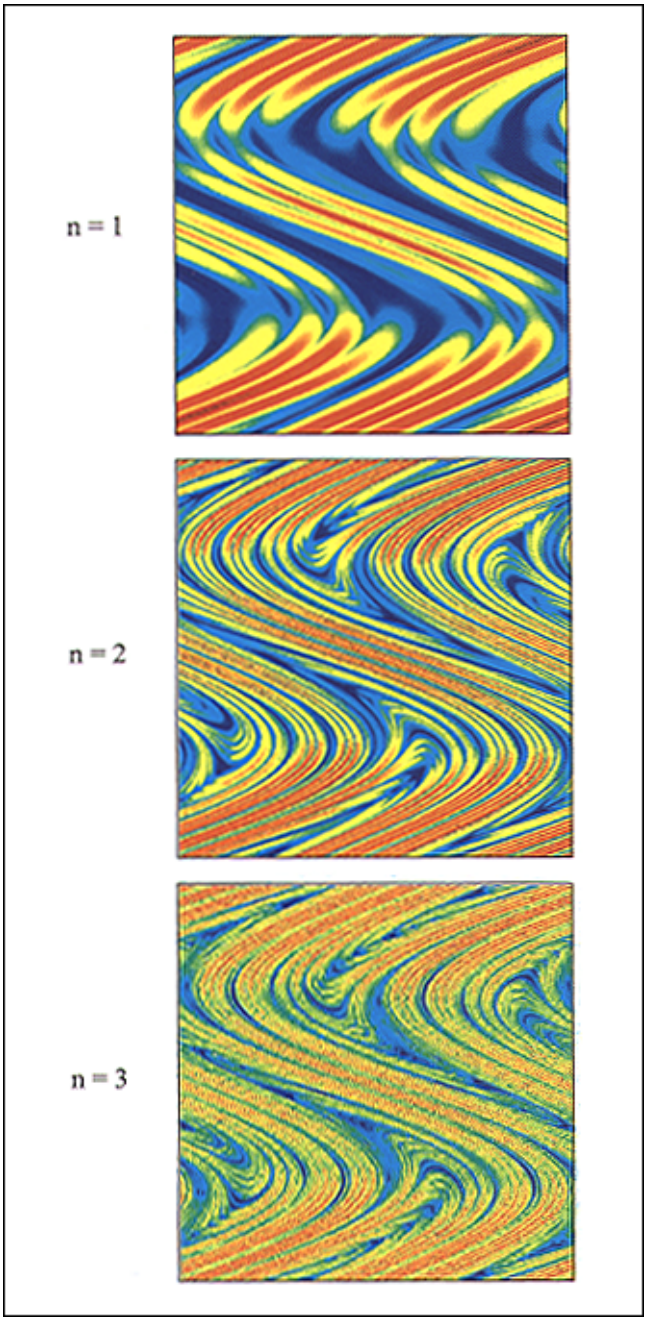

Figure 8. Stretching field in the sine flow with $T = 1.6$ after three consecutive periods, $n = 1$, 2, and 3.

The self-similarity of the stretching field is quantitatively demonstrated in Figure 9. We computed the probability density function of the stretching intensities for each period as

$$H(\log\lambda) = \frac{1}{N_P}\frac{dN(\log\lambda)}{d\log\lambda} \tag{8}$$

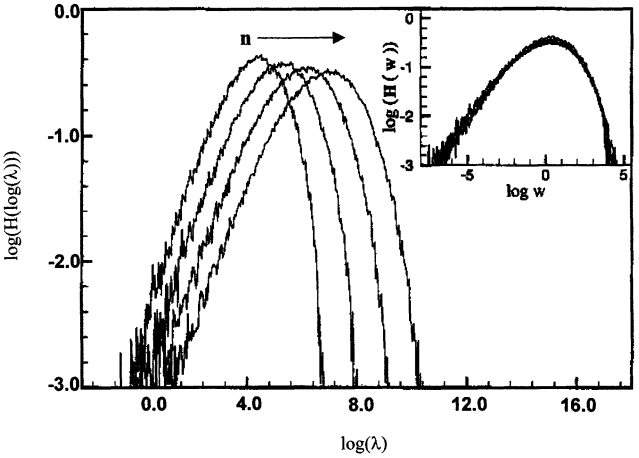

Figure 9. Probability distribution of stretching intensities, *pdf*[log(λ)], developing a characteristic, self-similar shape in a few flow periods.

Large figure indicates *pdf*[log(λ)] for $n = 5$, 6, 7 and 8. The inset shows the invariant curves after scaling by standardization.

where λ represents the accumulated stretching of a fluid element (In other work, $H(w)$ has been called $\Pi(\alpha)$ (Adrover, 1998)). $dN(\log\lambda)$ is the number of fluid elements that have stretching values between $(\log\lambda)$ and $(\log\lambda + d\log\lambda)$ and N_P is the total number of fluid elements whose stretching is computed. As time progresses, the distributions of $|(\log(\lambda)|$ broaden as the fluid filaments accumulate stretching from period to period. The broad statistical distribution of stretching values implies that the rate of micromixing due to convective flow is different at different locations in the flow. However, the self-similar shape of the distributions suggests that from a statistical viewpoint, the stretching process remains the same as time evolves. In order to examine the scaling behavior of stretching, we use standardization to define a new variable w. The scaling of $\log\lambda$ is performed by subtracting the mean $(\log\langle\lambda\rangle)$ and dividing by the standard deviation of $\log\lambda$ $(\sigma_{\log\lambda})$

$$w = \frac{\log\lambda - \langle\log\lambda\rangle}{\sigma_{\log\lambda}} \tag{9a}$$

The scaled distributions $(H(\log(w))$, shown in the inset of Figure 9, are computed as follows

$$H(\log(w)) = \frac{dN[\log(w)]}{d\log(w)} = \sigma_{\log\lambda} H(\log\lambda) \tag{9b}$$

The effective collapse over several flow periods indicates that the convective mixing process becomes a periodic multiplicative operator leading to the emergence of a self-similar stretching field. As we have shown elsewhere, the stretching field is characterized by an invariant topology determined by the global manifolds of the flow.

The invariance of the stretching field has important consequences for reactive flows. The stretching at each location within the flow is intimately related to the local striation thickness s, which is the width of the evolving mixing structure at that location of the flow and which determines the local diffusional length scale. As the fluid interface grows and is connected to different regions of the flow, each portion of the interface stretches according to the local stretching rate. It eventually samples the entire range of stretching intensities. Simultaneously, fluid filaments decrease in width proportionally to the stretching they experience. A broad distribution of striation thicknesses (STD) is created that is directly related to the spectrum of stretching intensities shown in Figure 9. Furthermore, the convective mixing process continuously creates intermaterial contact area in the flow, which determines the rate of interfacial diffusion at each location. The amount of intermaterial area at each location in the flow is measured by ρ, the intermaterial area density (IAD), which is the inverse of s and has a controlling influence on reactive processes. IAD determines the amount of interface available for transport in different portions of the fluid, and STD measures the distribution of length scales diffusion which must be overcome to achieve complete homogenization. In general, direct prediction of either s or ρ is very difficult. Fortunately, the distribution of s and ρ can be predicted from λ, and it is explained in detail elsewhere (Muzzio et al., 2000).

In this article we demonstrate that the stretching process holds the key role in the evolution of reactions in chaotic flows. The two most relevant quantities, the intermaterial area density and the striation thickness distribution, are controlled by the stretching process in chaotic flows. Let us first examine the convective mixing process in the sine flow *in the absence of reaction or diffusion*. Consider the evolution of the interface between two fluids in the sine flow.

Initially, we fill the left half of the unit box with fluid A and the right half with fluid B. The evolution of the fluid-fluid interface can be tracked in the chaotic flow by placing small vectors along the initial filament and computing their positions after each period from Eqs. 7a and 7b. The lefthand side of Figure 10 illustrates the shape and distribution of the filament after the first three periods, $n = 1$, 2 and 3. As the convective mixing process takes place, the interface is repeatedly stretched and folded by the flow and creates a lamellar structure that has largely similar characteristics to the experimental mixing structure seen in Figure 1. The topology created by both the real and the model flows is composed of thousands of striations with a wide range of thicknesses. The spatial structure of the striations is determined by the multiplicative stretching and folding process. A characteristic pattern emerges after $n = 1$ and it preserves its original features; that is, every fold and branch present at $n = 1$ and 2 is also present at $n = 3$. Since the flow is nearly globally chaotic, the interface grows exponentially in length and spreads throughout the entire chaotic space. The self-similar evolution of the mixing patterns in Figure 10 is caused by a field of orientations that is everywhere tangent to the global unstable manifold of the flow. This field of orientations reveals a property common to all chaotic flows, which we have called asymptotic directionality (AD) (Giona, 1999; Muzzio et al., 2000). The existence of the invariant field of orientations guarantees the self-similar evolution of stretching (shown in Figure 8), and the self-similarity in the distribution of intermaterial area (shown in Figure 10).

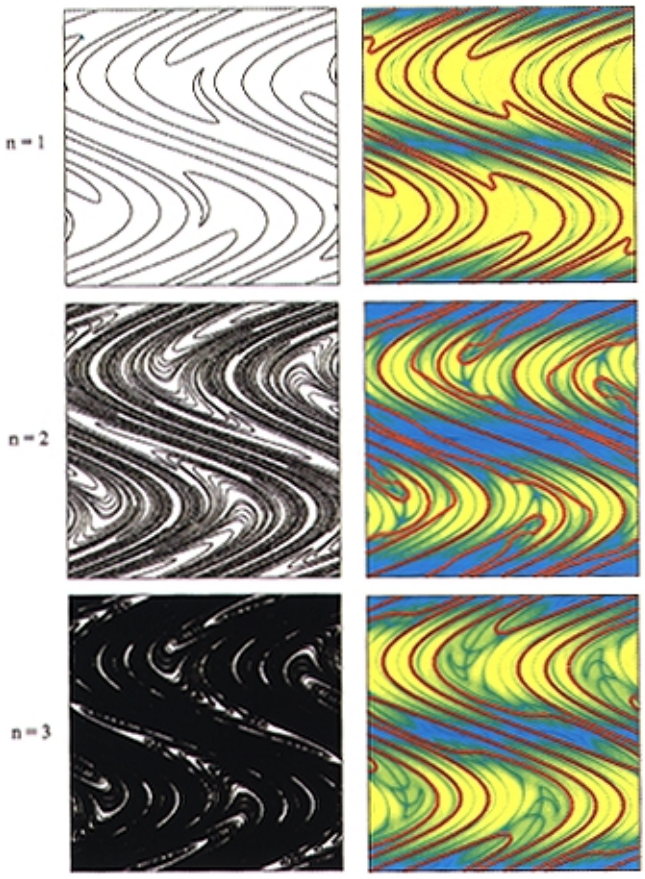

Figure 10. Distribution of intermaterial contact area in the sine flow with $T = 1.6$ after $n = 1$, 2 and 3 (left); rate of an instantaneous, bimolecular reaction ($A + B \rightarrow 2P$) in the same flow (right).

Hot zone, where the reaction proceeds very rapidly, is almost identical to the landscape of intermaterial contact area.

The effect of the AD property carries beyond the purely convective, becoming the central property controlling the topology of reactive regions. In order to demonstrate this point, let us consider what happens in the same chaotic system if diffusion and reaction occur along with convective mixing. The species balance equation in a dimensionless form for the flow with reaction, diffusion, and convection is

$$\frac{\partial c_i}{\partial t} + \bar{v} \cdot \nabla c_i = \frac{1}{Pe} \nabla^2 c_i + R_i \qquad (10)$$

where Pe, the Péclet number, measures the relative magnitude of the characteristic time for convection to diffusion. Applications usually have values of Pe in the range of 10^2 (laminar flames) to 10^{10} (turbulent reactive flows, polymerizations). For problems where convective mixing plays an important role, it is of interest to choose Pe as high as possible. If the two time scales were of the same order (that is, $Pe \cong 1$), mixing effects would be unimportant, because diffusion would erase heterogeneities as quickly as convection creates them. At the other end of the spectrum, where Pe is very high, diffusion is very slow compared to the convective mixing process. In this case, very fine, partially mixed structures remain intact for long times before diffusion has an effect. The spatial resolution (that is, maximum distance between neighboring nodes) that is necessary to capture the details of the mixing structure determines the upper bound of the Pe for practical applications. For the results presented in this article, given available computer resources, $Pe = 2{,}000$ is the highest practical value.

Similar to the analysis of the 1-D model discussed in the previous section, we consider a bimolecular reaction: $A + B \rightarrow 2P$ and define $\varphi = c_A - c_B$. For infinitely fast reactions, since A and B cannot coexist, a single equation describes both the reactant and product concentrations

$$\frac{\partial \varphi}{\partial t} + \bar{v} \cdot \nabla \varphi = \frac{1}{Pe} \nabla^2 \varphi \qquad (11)$$

In order to describe the evolution of φ, standard finite-difference methods were employed to solve Eq. 11 at ($1{,}024 \times 1{,}024$) nodes in the flow. Initially, half of the flow domain was filled with A and the other half contained only B (see Figure 7). The reactant and product concentrations are computed from φ according to Eq. 4.

Once the product concentration is known as a function of time, the local reaction rate can be determined from mass conservation

$$r = \frac{1}{2}\left(\frac{\partial c_P}{\partial t} + v \cdot \nabla c_P - D \nabla^2 c_P \right) \qquad (12)$$

Equation 12 in some sense captures the fact that three processes, the local reactivity, diffusive transport, and convective mixing, control the effective reaction rate. We now examine how each of these three components affect the overall evolution of a reactive mixing process.

The reaction rate after the first three periods of the sine flow with $T = 1.6$ is illustrated on the righthand side of Figure 10. The three figures represent r after $n = 1$, 2 and 3, so its time evolution can be followed from the top to the bottom of the figure. We use a logarithmic scale to illustrate the spatial variations of r. The colors are relative to the maximum rate after each period, which is 69.82 after $n = 1$, 25.70 after $n = 2$, and 4.81 after $n = 3$. The areas of highest rate (colored in red) represent the hot zones in the flow, where the instantaneous reaction occurs. The rapid decrease in the maximum rate shows how fast reactants are consumed by the reaction. During the first three periods, the reaction proceeds very rapidly: the conversion is 49.3% at $n = 1$, 87.7% at $n = 2$, and reaches 96.5% at $n = 3$.

Compare the lefthand side and righthand side columns of Figure 10, where the purely convective flow is compared with the reactive/diffusive case. The hot zones, where the reactive interface is, closely agree with the locations of highest filament density. The landscape of the nonreactive mixture (lefthand side of Figure 10) looks almost identical to the landscape of the reactive flow (righthand side of Figure 10). This similarity is not coincidental; the two sets of figures are

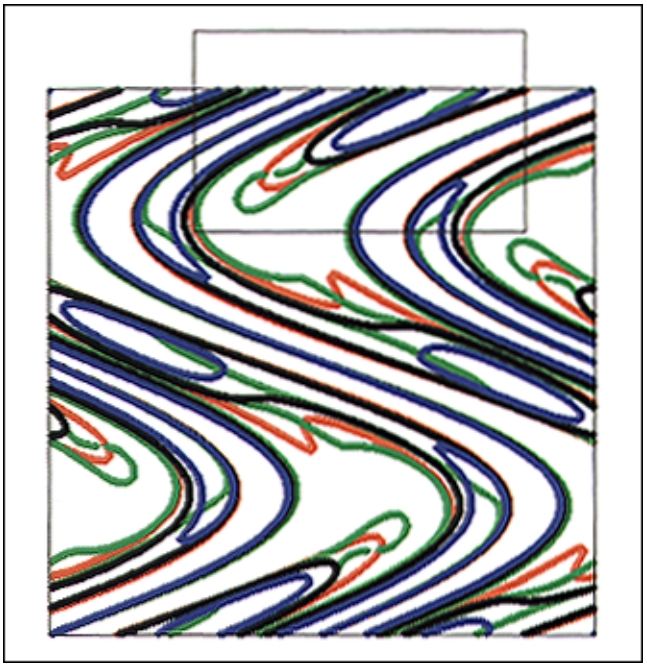

Figure 11. Time evolution of the reaction front in the sine flow with $T = 1.6$.

Four curves correspond to four consecutive periods: $n = 1$ (red); $n = 2$ (green); $n = 3$ (black); $n = 4$ (blue).

highly correlated. The stretching process is the sole determinant of where interface is created, and establishes where intimate contact between fluids A and B is achieved. Once the playing field is set by convective stretching, diffusion and reaction follows: the landscape of the reactive zone closely outlines the location of the fluid-fluid interface determined by the purely convective case. Diffusive transport in each region is proportional to ρ, the amount of interface at that location. The areas in the flow where striations contain only A or only B remain inactive, because no reaction takes place there. However, in the areas that contain neighboring striations of A and B (that is, areas where the A-B interface is), diffusion immediately transports material across the interface, the reaction proceeds, and product begins to accumulate.

There are some differences between the nonreactive and the reactive landscapes (in the lefthand side and righthand side columns of Figure 10). The thinnest striations contain the least amount of reactants, so they are consumed first by the reaction. As time progresses, these striations become exhausted and the reaction front advances. To illustrate this point, we superimposed the regions of highest reaction rate ("hot zones") at periodic intervals for four periods ($n = 1$ to 4) in Figure 11. Examine the movement of the reaction front in the enclosed box. Early on, convection creates new striations and more interface, so the reaction zone stretches (red to green). Then, it quickly reaches a balance with diffusion, and reaction proceeds until the area begins to run out of material. As a result, the reaction extinguishes and the hot zone migrates (black to blue). The interplay of the two mechanisms, creation of intermaterial area and diffusion, determine how fast striations are consumed by the reaction. The exponential stretching process controls both of these mechanisms.

Next, we examine the spatial distribution of reactants and products as they evolve in time. The lefthand side column of Figure 12 shows the spatial distribution of reactants after $n = 1$, 2 and 3. The righthand side column of Figure 12 is the corresponding product distribution in the flow. Similarly to previous contour plots, the colors of each figure are based on the relative maximum values of reactants and products, respectively. On the lefthand side, striations of A (red) interpenetrate striations of B (blue) and regions near the reactive interface quickly become exhausted. At the same time, the product appears at these locations, following the same landscape as in Figure 10. The initially thin product-rich filaments become increasingly thicker until isolated areas of low product concentration remain dispersed in the flow. These islands of low product concentration contain exclusively reactant A or B, as seen in the corresponding lefthand side picture. They remain intact until diffusion transports reactants to these regions from the surrounding striations.

As the reaction gradually progresses, the total amount of product changes in each location of the flow. Compared with the stretching field in Figure 8, where no diffusion or reaction affects the striations, the product concentration field looks increasingly blurred. Diffusion increasingly smears the boundaries of striations in Figure 12 and the two landscapes look increasingly different. However, the difference is primarily cosmetic. As shown in Figure 13, the product concentration field remains statistically self-similar. Using once again standardization, the product concentration after each period is scaled by the mean ($\langle \log c_P \rangle$) and the standard deviation ($\sigma_{\log c_P}$). The probability density function of c_P remains invariant over three flow periods after the distributions are collapsed according to Eqs. 9a and 9b. Note here that the conversion at the end of the 4th period, corresponding to the pink curve on the plot, is over 96%. By this time the reaction is close to completion; in fact, most areas have become exhausted of reactants, thus demonstrating that self-similar dynamics control the entire evolution of the reactive mixing process.

Onwards and Upwards: 3-D Systems

As this article demonstrates, convective mixing not only affects the progression of reactions in chaotic flows, but has governing control on their evolution. The idea must be abandoned that it is sufficient to have the end result in mind when designing a laminar reactive mixing process. The only route to fast mixing in laminar applications is via chaotic flows and the mixing intensity in these systems is inherently nonuniform. In such systems, a wide spectrum of stretching intensities distributes material interface along a pre-defined, invariant template. It establishes intimate contact between mixture components (whether reactive or not) and controls the local rate of diffusion through the intermaterial area density and striation thickness distribution. All chaotic mixing flows share these characteristics.

Understanding the interplay of the three mechanisms, reaction, diffusion and convection, is essential. In light of what happens in 2-D reactive chaotic flows, we can attempt to extend the analysis to 3-D reactive mixing applications. Let us

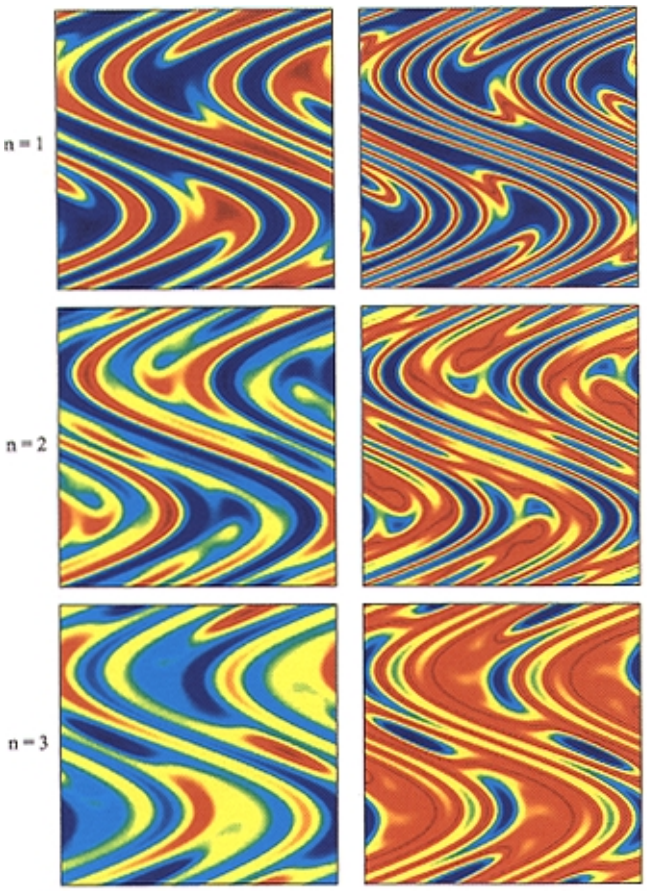

Figure 12. Concentration of reactants *A* and *B* after the first three flow periods in the sine flow with $T = 1.6$ (left); product concentration (right).

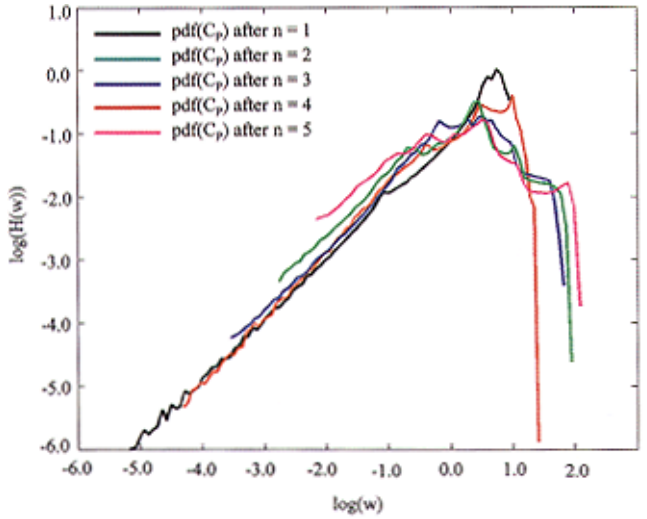

Figure 13. Probability density functions of product concentration collapse to an invariant distribution in the sine flow over three periods after standardization.

This behavior is the consequence of self-similarity in the concentration field.

take a fresh look at the 3-D, "real life" example considered earlier in this article. In Figure 1 we described one of the most common practical reactive flows, a stirred tank agitated by three Rushton turbines. Analytical solutions for stretching and particle positions, such as Eqs. 7a and 7b, are not available for 3-D flows, so we need to rely on numerical methods to compute the stretching and the filament structure. Figure 14 shows a dye filament, initially placed vertically near the impeller shaft, as it is stretched and folded into a complex mixing structure that eventually invades the entire chaotic region. The four pictures in the figure indicate four computational snapshots of the chaotic mixing process at consecutive times. The computational tools that we used for this work have been described and validated elsewhere (Zalc et al., 2001). We computed the structure of the filament by placing 200,000 tracer particles in a line along the shaft.

As time increases and convective mixing takes place, the material filament gradually invades portions of the chaotic region. A convoluted, partially mixed structure develops after 60 revolutions and the location of the filament marks the interface between the mixture components, as indicated in the last figure. An experiment using a pH-sensitive dye is compared to the last figure, where dye was initially injected near the impeller blades. A photograph after 60 impeller revolutions indicates that the filament acquires an identical structure in the experiments, as predicted by the computed mixing structure. Since the dye is pH sensitive, an instantaneous acid-base reaction occurs in the tank at the interface between the mixture components. The mechanism that controls the evolution of the reactive mixing process is largely the same as in the sine flow described earlier. The fluorescent, pH-sensitive dye gives a visual indication of the reaction zones, where the acid-base reaction occurs in the tank. The product-rich areas glow with high illumination, and its shape unmistakably coincides with the mixing structure created by the convective flow.

We can go further than qualitative comparisons, and compute the probability density function of the concentrations in the tank using Eq. 9. In order to measure the product concentrations experimentally, we developed an image analysis technique that quantifies the level of luminescence in the experimental photograph. The time-evolution of the reactive process is monitored by taking a series of pictures similar to the one in Figure 14d. Product concentration is quantified based on the pixel values in each photograph. Then, knowing the spatial distribution of the product, the same statistical tools are applied to compute the pdf(w). Figure 15 indicates the distribution of c_P in the three-impeller stirred tank at three different times. The evolution of the acid-base reaction 1, 2 and 3 min. after injecting the dye is captured during the experiments. In light of the self-similarity that occurs in 2-D reactive chaotic processes (recall Figure 13), we expect the scaled product concentration profiles to show an invariant distribution. Figure 15 confirms this expectation for the 3-D reactive flow. The distribution of the scaled concentration profiles after 1, 2 and 3 min. fall right on top of one another and also agree closely with the scaled distribution obtained from the 2-D model system. The agreement is shown in Figure 15 by overlaying the curve from $n = 3$ from the sine flow with the experimental data. This preliminary result suggests that self-similarity also appears in 3-D reactive flows, and im-

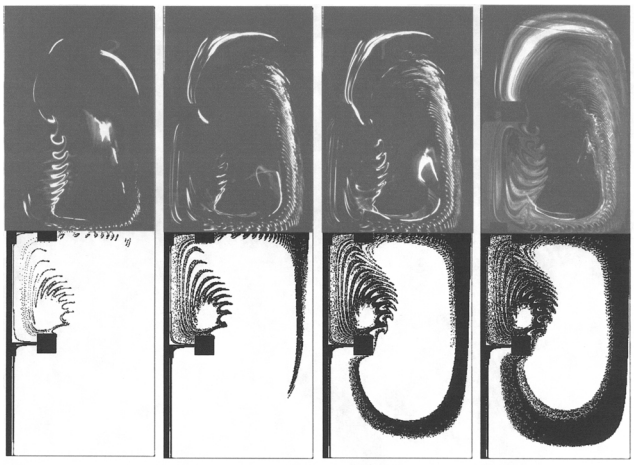

Figure 14. Evolution of a fast reaction in a mixing tank stirred with three Rushton impellers at *Re* = 20.

Reactive zones in a stirred tank is identical to the location of the intermaterial contact area in a mixing after 10, 20, 40 and 60 impeller revolutions. Each figure shows half of the vertical cross section, where the shaft and three impeller blades are seen on the lefthand side. Upper half shows the reactive flow and bottom is the computed chaotic mixing structure.

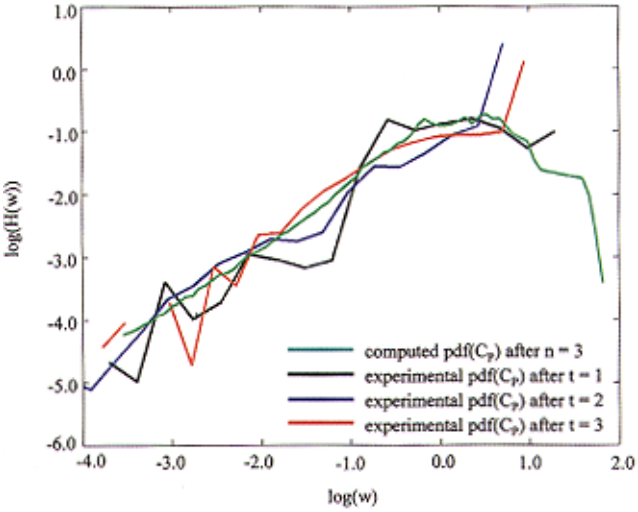

Figure 15. Probability density function of the product concentration in the tank calculated from the experimental images after *t* = 1, 2 and 3 min.

Experimental distributions in the 3-D chaotic flow are invariant after scaling and match the scaling of the model system as shown by overlaying the distribution from $n = 3$ from Figure 13.

plies that the chaotic stretching and orientation process governs the evolution of reactions in 3-D systems, indicating a clear conceptual direction pregnant with promise.

Conclusions

This article provides evidence that the stretching field in a chaotic flow has a controlling influence on reactive processes, when convection, reaction, and diffusion occur on the same time scale. First, using a 1-D example, we showed that the evolution of a single lamella is entirely determined by the stretching rate. Subsequently, using a 2-D chaotic flow where the reactive mass balance equations can be solved with high precision, we compared the behavior of the reactive flow with the nonreactive chaotic mixing process. We characterized the evolution of the mixing structure by stretching computations. Since stretching controls the location and density of the intermaterial area between reactive components, it has a direct impact on the rate of diffusion and reaction. As a result, the location of the reactive zones is practically identical to the mixing structure determined only by the chaotic stretching process. Furthermore, since stretching is a self-similar process, the distribution of product concentrations is self-similar as well and can be rendered invariant by statistical methods. Finally, when the same tools are extended to more complex reactive flows, such as flow in a stirred tank, we found that the statistical properties of the 3-D reactive flow were identical to the model system.

Further exploration of the connection between the stretching field and the reactive landscape can significantly extend our understanding of the fundamental relationship between reactions, diffusion, and convection. Computing the stretching and the location of the reactive material contact area is feasible in all chaotic flows, opening promising avenues for future work.

Literature Cited

Adrover, A., M. Giona, F. J. Muzzio, S. Cerbelli, and M. M. Alvarez, "Analytic Expression for the Short-Term Rate of Growth of the Intermaterial Contact Perimeter in Two-Dimensional Chaotic Flows and Hamiltonian Systems," *Phy. Rev. E*, **58**, 447 (1998).

Alvarez, M. M., F. J. Muzzio, S. Cerbelli, A. Adrover, and M. Giona, "Self-Similar Spatiotemporal Structure of Intermaterial Boundaries in Chaotic Flows," *Phys. Rev. Lett.*, **81**, 3395 (1998).

Angst, W., J. R. Bourne, and R. N. Sharma, "Mixing and Fast Chemical Reaction: V: Influence of Diffusion within the Reaction Zone on Selectivity," *Chem. Eng. Sci.*, **37**, 1259 (1982).

Avalosse, T. C., and M. J. Crochet, "Finite-Element Simulation of Mixing: 1. Two-Dimensional Flow in Periodic Geometry," *AIChE J.*, **43**, 577 (1997).

Chella, R., and J. M. Ottino, "Conversion and Selectivity Modifications due to Mixing in Unpremixed Reactors," *Chem. Eng. Sci.*, **39**, 551 (1984).

Crank, J., *The Mathematics of Diffusion*, Clarendon Press, Oxford (1956).

Fields, S. D., and J. M. Ottino, "Effect of Striation Thickness Distribution on the Course of an Unpremixed Polymerization," *Chem. Eng. Sci.*, **42**, 459 (1987).

Galfi, L., and Z. Racz, "Properties for the Reaction Front in an A + B ⇒ C Type Reaction-Diffusion Process," *Phys. Rev. A*, **38**, 3151 (1988).

Giona, M., A. Adrover, F. J. Muzzio, S. Cerbelli, and M. M. Alvarez, "The Geometry of Mixing in Time-Periodic Chaotic Flows: I. Asymptotic Directionality in Physically Realizable Flows and Global Invariant Properties," *Phys. D*, **132**, 298 (1999).

Hobbs, D. M., P. D. Swanson, and F. J. Muzzio, "Numerical Characterization of Low Reynolds Number Flow in the Kenics Static Mixer," *Chem. Eng. Sci.*, **52**, 1 (1997).

Kusch, H. A., and J. M. Ottino, "Analysis of Impingement Mixing-Reaction Data: Use of a Lamellar Model to Generate Fluid Mixing Information," *Ind. Eng. & Chem. Res.*, **28**, 302 (1989).

Lamberto, D. J., F. J. Muzzio, and P. D. Swanson, "Using Time-Dependent RPM to Enhance Mixing in Stirred Vessels," *Chem. Eng. Sci.*, **51**, 733 (1996).

Metcalfe, G., and J. M. Ottino, "Autocatalytic Processes in Mixing Flows," *Phys. Rev. Lett.*, **72**, 2875 (1994).
Muzzio, F. J., M. M. Alvarez, S. Cerballi, M. Giona, and A. Adrover, "The Intermaterial Area Density Generated by Time- and Spatially Periodic 2-D Chaotic Flows," *Chem. Eng. Sci.*, **55**, 1497 (2000).
Muzzio, F. J., and M. Liu, "Chemical Reactions in Chaotic Flows," *Chem. Eng. J.*, **64**, 117 (1996).
Muzzio, F. J., and J. M. Ottino, "Diffusion and Reaction in a Lamellar System: Self-Similarity with Finite Rates of Reaction," *Phys. Rev. Lett.*, **42**, 5873 (1990).
Muzzio, F. J., and J. M. Ottino, "Coagulation in Chaotic Flows," *Phys. Rev. A*, **38**, 2516 (1988).
Muzzio, F. J., and J. M. Ottino, "Dynamics of a Lamellar System with Diffusion and Reaction: Scaling Analysis and Global Kinetics," *Phys. Rev. A*, **40**, 7182 (1989a).
Muzzio, F. J., and J. M. Ottino, "Evolution of a Lamellar System with Diffusion and Reaction: A Scaling Approach," *Phys. Rev. Lett.*, **63**, 47 (1989b).
Neufeld, Z., and T. Tel, "The Vortex Dynamics Analogue of the Restricted Three-Body Problem: Advection in the Field of Three Identical Point Vortices," *J. Phys. A*, **30**, 2263 (1997).
O'Shaughnessy, B., and D. Vavylonis, "Interfacial Reactions: Mixed Order Kinetics and Segregation Effects," *Phys. Rev. Lett.*, **84**, 3193 (2000).
Ottino, J. M., "Description of Mixing with Diffusion and Reaction in Terms of the Concept of Material Surfaces," *J. of Fluid Mech.*, **114**, 83 (1982).
Ottino, J. M., "Mixing and Chemical Reactions. A Tutorial," *Chem. Eng. Sci.*, **49**, 4005 (1994).
Ottino, J. M., W. E. Ranz, and C. W. Macosco, "A Lamellar Model for Analysis of Liquid Liquid Mixing," *Chem. Eng. Sci.*, **34**, 877 (1979).
Ranz, W. E., "Applications of a Stretch Model to Mixing, Diffusion, and Reaction in Laminar and Turbulent Flows," *AIChE J.*, **25**, 41 (1979).
Rothstein, D., E. Henry, and J. P. Gollub, "Persistent Patterns in Transient Chaotic Fluid Mixing," *Nature*, **401**, 770 (1999).
Schenkel, A., P. Wittwer, and J. Stubbe, "Asymptotics of Solutions in an $A+B \Rightarrow C$ Reaction-Diffusion System," *Phys. D*, **69**, 135 (1993).
Sokolov, I. M., P. Argyrakis, and A. Blumen, "The $A+B \Rightarrow 0$ Reaction under Short-Range Interactions," *J. Phys. Chem.*, **98**, 7256 (1994).
Sokolov, I. M., and A. Blumen, "Distribution of Striation Thicknesses in Reacting Lamellar Systems," *Phys. Rev. A*, **43**, 6545 (1991).
Sokolov, I. M., and A. Blumen, "Diffusion-Controlled Reactions in Nonstoichiometrical Layered Systems," *Phys. A*, **191**, 177 (1992).
Szalai, E. S., and F. J. Muzzio, "Using CFD to Optimize the Design of Static Mixers," *AIChE J.*, in press (2002).
Taitelbaum, H., S. Havlin, J. Kiefer, B. Trus, and G. Weiss, "Some Properties of the $A+B \Rightarrow C$ Reaction-Diffusion System with Initially Separated Components," *J. of Stat. Phys.*, **65**, 873 (1991).
Taitelbaum, H., Y. Lee Koo, S. Havlin, R. Kopelman, and G. Weiss, "Exotic Behavior of the Reaction Front in the $A+B \Rightarrow C$ Reaction-Diffusion System," *Phys. Rev. A*, **46**, 2151 (1992).
Taitelbaum, H., B. Vilensky, A. Lin, A. Yen, Y. Lee Koo, and R. Kopelman, "Competing Reactions with Initially Separated Components," *Phys. Rev. Lett.*, **77**, 1640 (1996).
Unger, D. R., and F. J. Muzzio, "Laser-Induced Fluorescence Technique for the Quantification of Mixing in Impinging Jets," *AIChE J.*, **45**, 2477 (1999).
Zalc, J. M., and F. J. Muzzio, "Parallel-Competitive Reactions in a Two-Dimensional Chaotic Flow," *Chem. Eng. Sci.*, **54**, 1053 (1999).
Zalc, J. M., M. M. Alvarez, B. E. Arik, and F. J. Muzzio, "Extensive Validation of Computed Laminar Flow in a Stirred Tank With Three Rushton Turbines," *AIChE J.*, **47**, 2144 (2001).

Manuscript received Mar. 22, 2002, and revision received July 31, 2002.